

Shot-to-shot diagnostic of the longitudinal photon source position at the SPring-8 Angstrom Compact Free Electron Laser by means of x-ray grating interferometry

YVES KAYSER,^{1,*} SIMON RUTISHAUSER,¹ TETSUO KATAYAMA,² TAKASHI KAMESHIMA,² HARUHIKO OHASHI,² UWE FLECHSIG,¹ MAKINA YABASHI,³ AND CHRISTIAN DAVID¹

¹Paul Scherrer Institut, 5232 Villigen-PSI, Switzerland

²Japan Synchrotron Radiation Research Institute, Kouto 1-1-1, Sayo-cho, Sayo-gun, Hyogo 679-5198, Japan

³RIKEN SPring-8 Center, 1-1-1 Kouto, Sayo-cho, Sayo-gun, Hyogo 679-5148, Japan

*Corresponding author: yves.kayser@psi.ch

Received 30 November 2015; revised 12 January 2016; accepted 12 January 2016; posted 13 January 2016 (Doc. ID 254754); published 5 February 2016

We present single-shot measurements of the longitudinal photon source position of the SPring-8 Angstrom Compact Free Electron Laser x-ray free electron laser by means of x-ray grating interferometry. The measurements were performed in order to study the behavior of the source under normal operation conditions and as a dependence on the active undulator length. The retrieved experimental results show that x-ray grating interferometry is a powerful *in situ* monitoring tool for investigating and tuning an x-ray free electron laser. © 2016 Optical Society of America

OCIS codes: (050.1950) Diffraction gratings; (120.0120) Instrumentation, measurement, and metrology; (140.2600) Free-electron lasers (FELs); (340.7450) X-ray interferometry.

<http://dx.doi.org/10.1364/OL.41.000733>

At synchrotron radiation facilities, x-ray grating interferometry (XGI) has become an established technique for imaging applications (e.g., Refs. [1–7]) and wavefront sensing measurements [8–14]. Indeed, this technique allows for *in situ* investigations of the wavefront gradient with an experimentally demonstrated accuracy of the order of tens of nanoradians [14,15]. At x-ray free electron laser (XFEL) facilities, the stochastic nature of the self-amplified spontaneous emission (SASE) complicates the wavefront analysis. Nevertheless, XGI proved to be an adequate tool for the at-wavelength investigations of mirror and monochromator properties in order to study their impact on the wavefront [16,17]. In the present study, XGI is used to explore on a single-shot basis the longitudinal photon source position of the SPring-8 Angstrom Compact Free Electron Laser (SACLA) [18] in the normal operation mode and as a dependence on the active undulator length. The retrieved information is of interest for tuning the machine and provides information on the stability. Thus, it can contribute to a better understanding of the lasing process and XFEL facilities in general.

In an XGI experiment (Fig. 1), the incident x-ray beam is diffracted by a periodic binary structure. The interference between the x-ray beams corresponding to the positive and negative diffraction orders results further downstream of the grating in intensity modulations. The periodic binary structure, the grating, is in the one-dimensional version a line structure and in the two-dimensional version a mesh pattern structure. Typically, the diffraction grating is optimized to yield the best diffraction efficiency in the ± 1 st diffraction order (duty cycle 0.5, π -phase shift), and the periodicity of the grating is in the micrometer range [19]. For this configuration, the resulting constructive interference pattern, at the odd-numbered fractional Talbot orders (where the contrast is the best), will present, for plane waves, a periodicity which is half the periodicity of the diffraction grating. Most position-sensitive detectors do not have sufficient resolution to spatially resolve the interference pattern. Therefore, a second grating with absorbing lines having the same periodicity as the interference pattern, is positioned in front of the detector. The interference pattern can then be resolved by aligning the structures of the absorption grating with the interference fringes followed by a spatial scan of one of the gratings in order to acquire a position-dependent intensity pattern (phase-stepping mode). Alternatively, the absorption grating is deliberately misaligned with respect to

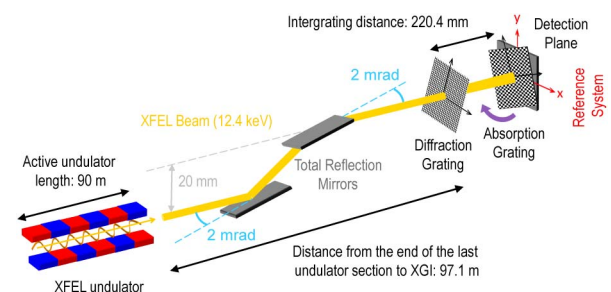


Fig. 1. Schematic of the setup used during the experiment.

the interference pattern produced by the diffraction grating in order to generate a moiré pattern (moiré mode). The moiré pattern can be described by $I_m = \cos(2\pi x/p_{mx} + 2\pi y/p_{my})$, with p_m representing the periodicity of the moiré pattern in the horizontal (x) and vertical (y) direction [16]. It is the result of the superposition of the self-image of the first grating with the absorbing structures of the second grating. Its period depends on the relative angular alignment of the two gratings around the optical axis. The angle between the gratings can be tuned to give dense fringes for high spatial resolution or coarse fringes for high sensitivity of the measurement. The moiré mode benefits from a lower sensitivity to magnification issues which either result in residual moiré fringes or require to be accounted for in the grating design phase before it is produced. The main advantage of the moiré mode is its single-shot capability allowing one to investigate the wavefront of each individual pulse with a sensitivity of the order of tens of nanoradians when performing measurements at XFEL facilities.

The XGI measurements at the SACLA were realized at a photon energy of 12.4 keV and the machine was operated at a repetition rate of 10 Hz. The pulse energy was monitored by an in-line beam monitor [20,21] and fluctuated between 140 and 150 μJ ($\approx 7.5 \times 10^{10}$ photons). The nominal values of the peak current, the bunch duration, and the normalized projected emittance of the electron beam were 3.5 kA, 20 fs in FWHM, and 1 π mm mrad, respectively [18], while that of the XFEL pulse duration was ~ 10 fs [22]. The grating interferometer (see Fig. 1) was installed in the experimental hutch 1 of beamline 3 at 97.1 m from the end of the undulator and operated in the 11th Talbot order. One- and two-dimensional gratings were used during the experiment. The moiré patterns were recorded using a 2D camera system coupled to a YAG screen (effective pixel size: 3.83 μm). The diffraction gratings had a periodicity of 4 μm , a duty cycle of 0.5, and a structure height chosen such as to generate a π phase shift. The absorption grating had hence a periodicity of 2 μm . The grating patterns were written by electron beam lithography with an electron beam writer using the continuous path mode in order to ensure an accurate positioning of the structures [23]. Indeed, any grating distortion has a direct impact on the experimental results. The patterns were transferred into thinned Si wafers using a deep reactive ion etching process [24,25]. For the absorption grating, the trenches between the silicon structures were filled with gold by electroplating.

For quantitative results in the moiré mode, the angular orientation around the optical axis of the structures of both gratings has to be calibrated with respect to the camera system (see also Ref. [16]). This was realized by acquiring the moiré pattern sequentially at different angular positions of the absorption grating. Subsequently, the fringe frequency in the vertical and horizontal directions is extracted at each grating position using a two-dimensional fast Fourier transform (FFT) in order to calibrate the angular positions using a minimization procedure [12,26]. Furthermore, the radius of curvature (ROC) of the wavefront can be calculated from the information obtained via the minimization procedure [12,26]. Once the orientation of the grating structures is known, each recorded moiré pattern can be investigated individually via Fourier analysis [27]. As described in Ref. [16], a FFT is applied to the moiré pattern in combination with a Hann window to reduce boundary artifacts. The first-order component of the FFT is separated from the remaining frequencies using a bandpass filter (box window).

An inverse FFT of the isolated first-order component provides the fringe phase. After an unwrapping procedure [28], the wavefront phase and propagation angles can be calculated using the information from the calibration procedure (Fig. 2) [16]. In the case of line gratings, one-dimensional forward and inverse FFT are calculated in the direction transverse to the moiré fringe pattern, while in the case of mesh-patterned gratings two-dimensional FFTs are used. In the two-dimensional case, the first-order components are first isolated individually in each direction before the inverse FFT is calculated separately for both components in order to retrieve the fringe phase individually in the horizontal and vertical directions, respectively. The ROC of the incident wavefront can be either calculated from the fringe phase [17,29] or equivalently it can be retrieved from the slope of the wavefront propagation angle (as defined in Ref. [16]):

$$\text{ROC}_x = \frac{d}{M-1} = d / \left(\frac{M_0 \sin \beta_1}{\sin \beta_2 - p_2/p_{m,x}} - 1 \right),$$

$$\text{ROC}_y = d / \left(\frac{M_0 \cos \beta_1}{\cos \beta_2 - p_2/p_{m,y}} - 1 \right), \quad (1)$$

where d is the distance between the diffraction and absorption gratings, M_0 is the design magnification of the interferometer, β_1 and β_2 are the rotation angles of the diffraction and absorption gratings relative to the camera coordinate system around the beam axis, respectively, and p_2 is the period of the absorption grating.

If the wavefront is not perturbed by an x-ray optical element, the retrieved ROC is a measure of the source position along the beam propagation axis from the location of the

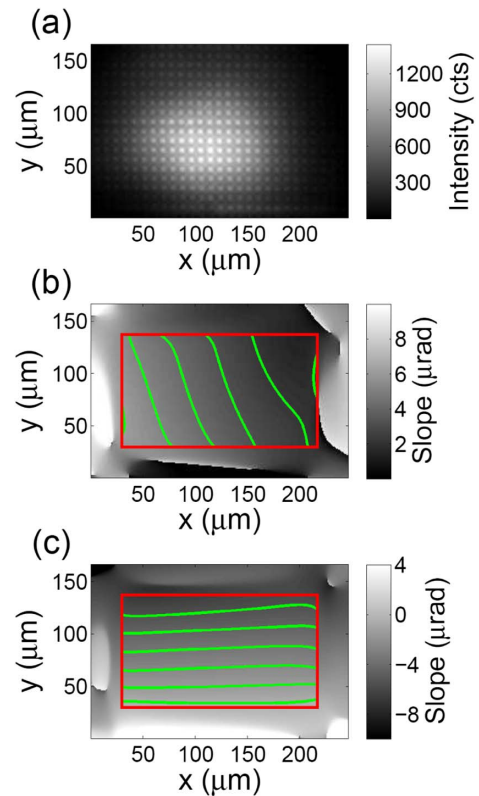


Fig. 2. (a) Two-dimensional moiré pattern and the wavefront slopes in the (b) horizontal and (c) vertical directions. The ROCs of the wavefront were extracted from the central part only (red rectangle) to exclude regions with low intensity.

grating interferometer. For the measurements at the SACLA a vertically deflecting pair of total reflection mirrors [30] was used upstream of the x-ray grating interferometer. Assuming that the vertically deflecting x-ray optics do not distort the horizontal component of the wavefront, the horizontal ROC corresponds to the longitudinal photon source position. The longitudinal source position and its evolution were studied on a shot-to-shot basis during two types of measurements which are discussed hereafter.

In the first experiment, the moiré patterns were recorded for each individual pulse produced by the SACLA over a time lapse of 5 h. The full available active undulator length (90 m) was used for the lasing process. During the measurements in 18 of the 19 available undulator sections (length 6.15 m) an undulator (length of the array of dipole magnets is 5 m) was installed. No undulator was installed in section 9 at the time of the measurements. A calibration measurement before and after the long-term study confirmed the stability of the grating interferometer. Both calibration measurements yielded the same results in terms of angular orientation of the gratings and ROC within the uncertainties of the fitting algorithm. Thus, the gratings showed no alteration or degradation when exposed to the SACLA pulses over several hours. The measurements were realized with two-dimensional gratings which allowed us to acquire information in the horizontal and vertical direction simultaneously. The evolution of the horizontal and vertical ROC was investigated by analyzing each 10th XFEL pulse recorded over the 5 h time lapse, corresponding to a sampling rate of 1 Hz, and by investigating the averaged image of 10 consecutive pulses, i.e., the averaged horizontal and vertical ROC over 1 s in order to be less sensitive to shot-to-shot fluctuations.

The retrieved horizontal and vertical ROC jittered around respective centroid values of 159.7 ± 0.1 m and 67.7 ± 0.1 m (see Fig. 3, fitted values from the histograms). These values are in-line with the results from the two calibration measurements for which the returned results for the horizontal and vertical ROC were 159.4 ± 3.0 m and 160.2 ± 3.0 m and 73.5 ± 0.6 m and 72.8 ± 0.6 m, respectively. The results show that the vertically deflecting total reflection mirrors have a strong impact on the vertical component of the wavefront. The horizontal ROC indicates, on the other hand, that the longitudinal photon source position is approximately 62.6 m upstream from the end of the undulator, i.e., about 10 undulator sections. The histogram of the horizontal and vertical ROC present a standard

deviation of 7.5 m with a skewness toward larger values and 1.8 m. The values for the centroid positions and the widths of the histogram were confirmed when investigating regularly spaced intervals of 1000 consecutive pulses from the SACLA machine, the different intervals being spaced by 10,000 pulses. The shape of the distribution did thus not change throughout the measurement. The mean values from the statistical analysis of the different histograms agree with the investigation of the 5 h interval. The temporal evolution of the horizontal ROC presents a slightly decreasing trend of the horizontal ROC (thus, the longitudinal photon source position) from about 165 m to about 155 m during the first 50 min followed by an increase to about 160 m in the following 20 min (Fig. 3, lower left panel). Afterward, the horizontal ROC jitters around a value range spanning from 159 to 161 m and is thus roughly stable except for a few sudden jumps of the centroid value when the lasing of the machine was not successful for a series of consecutive pulses. The vertical ROC, on the other hand, does not present any trend and jitters throughout the monitored time interval around the centroid value extracted from its histogram (Fig. 3, upper panels). This agrees with the fact the vertical ROC is essentially defined by the vertically deflecting mirrors. Furthermore, no correlation over time between the horizontal ROC, the vertical ROC, the mean photon energy, and the pulse energy could be observed.

In a second experiment, the active undulator length was changed by opening successively the undulator gaps between the measurements starting from the most downstream undulator and moving upstream while leaving the gaps of downstream undulators opened. This study was intended to explore the gain regime in terms of movement of the longitudinal photon source position of the SACLA. Between each change in the active undulator length, a calibration measurement was performed followed by the acquisition of the single-shot moiré pattern for 1000 individual XFEL pulses at a fixed position of the gratings. This allowed for cross-checking the grating interferometer itself between successive measurements as well as the ROC retrieved from the calibration measurement and the consecutive single-shot measurements. Since only the variation in the horizontal ROC is of interest, this study was performed with one-dimensional gratings with vertically aligned grating lines. The pulse energy was recorded simultaneously using an intensity monitor upstream of the total reflection mirrors [20,21].

From the evolution of the horizontal ROC with the active undulator length, three different regimes for the longitudinal photon source position can be identified (Fig. 4). When decreasing the active undulator length, the longitudinal source position remains at first between the ends of the 8th and 9th undulator section, thus confirming the results obtained with the two-dimensional gratings. The changes in the horizontal ROC when varying the active undulator length by opening the gaps of the four most downstream undulators correspond to less than an undulator section. This indicates that the XFEL is saturated and that the lasing of the machine is realized within the first 80 m, an observation which is also confirmed by the measured pulse energy. When the active undulator length is reduced to smaller values by opening successively the gaps of the next four undulators, the horizontal ROC starts to increase toward larger values. This means that the longitudinal photon source position moves upstream as well, and the change in source position follows furthermore the reduction in the active undulator length. Indeed, the distance between the source position and the end of

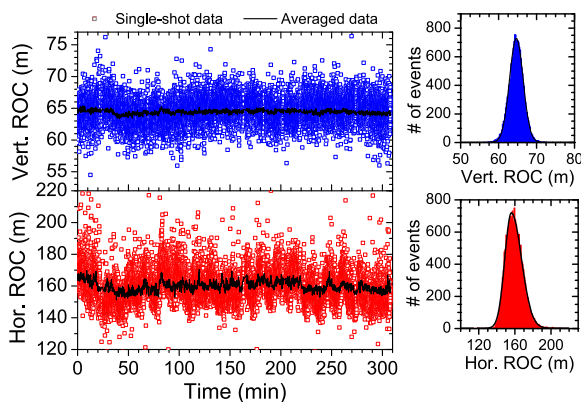


Fig. 3. Temporal evolution of the horizontal and vertical ROC followed at a 1 Hz rate over a time lapse of 5 h (left panels) and the corresponding histograms (right panels).

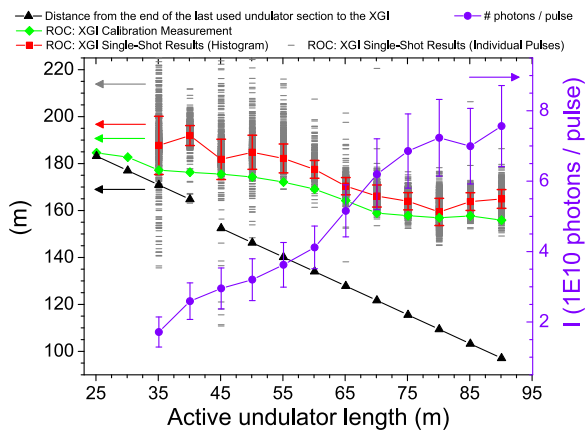


Fig. 4. Evolution of the pulse energy as measured by a beam intensity monitor and of the horizontal ROC according to the calibration measurements and the single-shot data evaluation as a function of the active undulator length. The distribution of the single-shot data points are shown as well as the centroid (red points) and width of the distribution (error bars).

the last used undulator section is constant within the length of an undulator section. In this regime, the monitored pulse energy also scales linearly with the active undulator length. Finally, when further decreasing the active undulator length, the horizontal ROC increases and the pulse energy decreases at a smaller rate. The longitudinal photon source position approaches the end of the last active undulator section. Moreover, the spread of the horizontal ROC retrieved from the single-shot moiré pattern evaluation increases considerably due to limitations imposed by the decreasing photon statistics on the detector. Throughout the scan of the active undulator length, XGI and the intensity monitor allowed us to draw the same conclusion about the saturation behavior of the SACLA machine. Indeed, a negative linear correlation can be found between the retrieved horizontal ROC and the measured pulse energy. From the XGI calibration scans, which confirmed the trend from the single-shot measurements although smaller radii of curvature were found, the horizontal ROC could be extracted for even smaller active undulator lengths since averaged images were considered in the data evaluation.

In summary, single-shot measurements at the SACLA of the longitudinal photon source position by means of XGI were presented. The longitudinal source position is equal to the horizontal ROC, which was measured on a shot-to-shot basis, assuming that the vertically deflecting x-ray optics do not distort the horizontal component of the wavefront. The temporal stability of the longitudinal photon source position in terms of position stability and jitter was established over a time lapse of 5 h. Moreover, the evolution of the horizontal ROC could be followed as a function of the active undulator length in order to establish the longitudinal photon source position in the gain and saturation regimes. Thus, it was demonstrated that XGI presents a valuable diagnostic tool with the potential to contribute to a better understanding of XFEL facilities and the produced pulses.

REFERENCES

1. A. Momose, W. Yashiro, H. Maikusa, and Y. Takeda, *Opt. Express* **17**, 12540 (2009).
2. S. A. McDonald, F. Marone, C. Hintermüller, G. Mikuljan, C. David, F. Pfeiffer, and M. Stupanoni, *J. Synchrotron Radiat.* **16**, 562 (2009).
3. T. Weitkamp, C. David, O. Bunk, J. Bruder, P. Cloetens, and F. Pfeiffer, *Eur. J. Radiol.* **68**, S13 (2008).
4. A. Momose, W. Yashiro, Y. Takeda, Y. Suzuki, and T. Hattori, *Jpn. J. Appl. Phys.* **45**, 5254 (2006).
5. T. Weitkamp, A. Diaz, C. David, F. Pfeiffer, M. Stupanoni, P. Cloetens, and E. Ziegler, *Opt. Express* **13**, 6296 (2005).
6. A. Momose, S. Kawamoto, I. Koyama, Y. Hamaiishi, K. Takai, and Y. Suzuki, *Jpn. J. Appl. Phys.* **42**, L866 (2003).
7. C. David, B. Nöhammer, H. H. Solak, and E. Ziegler, *Appl. Phys. Lett.* **81**, 3287 (2002).
8. H. Wang, K. Sawhney, S. Berujon, J. Sutter, S. G. Alcock, U. Wagner, and C. Rau, *Opt. Lett.* **39**, 2518 (2014).
9. S. Rutishauser, A. Rack, T. Weitkamp, Y. Kayser, C. David, and A. T. Macrander, *J. Synchrotron Radiat.* **20**, 300 (2013).
10. H. Wang, S. Berujon, I. Pape, S. Rutishauser, C. David, and K. Sawhney, *Opt. Lett.* **38**, 827 (2013).
11. H. Wang, S. Berujon, I. Pape, S. Rutishauser, C. David, and K. Sawhney, *Nucl. Instrum. Meth. A* **710**, 78 (2013).
12. H. Wang, K. Sawhney, S. Berujon, E. Ziegler, S. Rutishauser, and C. David, *Opt. Express* **19**, 16550 (2011).
13. S. Rutishauser, I. Zanette, T. Weitkamp, T. Donath, and C. David, *Appl. Phys. Lett.* **99**, 221104 (2011).
14. T. Weitkamp, B. Nöhammer, A. Diaz, C. David, and E. Ziegler, *Appl. Phys. Lett.* **86**, 054101 (2005).
15. C. David, S. Rutishauser, M. Sprung, I. Zanette, and T. Weitkamp, *AIP Conf. Proc.* **1466**, 23 (2012).
16. Y. Kayser, S. Rutishauser, T. Katayama, H. Ohashi, T. Kameshima, U. Flechsig, M. Yabashi, and C. David, *Opt. Express* **22**, 9004 (2014).
17. S. Rutishauser, L. Samoylova, J. Krzywinski, O. Bunk, J. Grünert, H. Sinn, M. Cammarata, D. M. Fritz, and C. David, *Nat. Commun.* **3**, 947 (2012).
18. T. Ishikawa, H. Aoyagi, T. Asaka, Y. Asano, N. Azumi, T. Bizen, H. Ego, K. Fukami, T. Fukui, Y. Furukawa, S. Goto, H. Hanaki, T. Hara, T. Hasegawa, T. Hatsui, A. Higashiya, T. Hirono, N. Hosoda, M. Ishii, T. Inagaki, Y. Inubushi, T. Itoga, Y. Joti, M. Kago, T. Kameshima, H. Kimura, Y. Kirihiro, A. Kiyomichi, T. Kobayashi, C. Kondo, T. Kudo, H. Maesaka, X. M. Maréchal, T. Masuda, S. Matsubara, T. Matsumoto, T. Matsushita, S. Matsui, M. Nagasono, N. Nariyama, H. Ohashi, T. Ohata, T. Ohshima, S. Ono, Y. Otake, C. Saji, T. Sakurai, T. Sato, K. Sawada, T. Seike, K. Shirasawa, T. Sugimoto, S. Suzuki, S. Takahashi, H. Takebe, K. Takeshita, K. Tamasaku, H. Tanaka, R. Tanaka, T. Tanaka, T. Togashi, K. Togawa, A. Tokuhisa, H. Tomizawa, K. Tono, S. Wu, M. Yabashi, M. Yamaga, A. Yamashita, K. Yanagida, C. Zhang, T. Shintake, H. Kitamura, and N. Kumagai, *Nat. Photonics* **6**, 540 (2012).
19. T. Weitkamp, I. Zanette, F. Pfeiffer, and C. David, *AIP Conf. Proc.* **1466**, 84 (2012).
20. K. Tono, T. Togashi, Y. Inubushi, T. Sato, T. Katayama, K. Ogawa, H. Ohashi, H. Kimura, S. Takahashi, K. Takeshita, H. Tomizawa, S. Goto, T. Ishikawa, and M. Yabashi, *New J. Phys.* **15**, 083035 (2013).
21. M. Kato, T. Tanaka, T. Kurosawa, N. Saito, M. Richter, A. A. Sorokin, K. Tiedtke, T. Kudo, K. Tono, M. Yabashi, and T. Ishikawa, *Appl. Phys. Lett.* **101**, 023503 (2012).
22. Y. Inubushi, K. Tono, T. Togashi, T. Sato, T. Hatsui, T. Kameshima, K. Togawa, T. Hara, T. Tanaka, H. Tanaka, T. Ishikawa, and M. Yabashi, *Phys. Rev. Lett.* **109**, 144801 (2012).
23. C. David and D. Hambach, *Microelectron. Eng.* **46**, 219 (1999).
24. S. Rutishauser, M. Bednarzik, I. Zanette, T. Weitkamp, M. Börner, J. Mohr, and C. David, *Microelectron. Eng.* **101**, 12 (2013).
25. C. David, J. Bruder, T. Rohbeck, C. Grünzweig, C. Kottler, A. Diaz, O. Bunk, and F. Pfeiffer, *Microelectron. Eng.* **84**, 1172 (2007).
26. S. Rutishauser, "X-ray grating interferometry for imaging and metrology," Ph.D. thesis (ETH Zurich, 2013).
27. M. Takeda, H. Ina, and S. Kobayashi, *J. Opt. Soc. Am.* **72**, 156 (1982).
28. M. A. Herráez, D. R. Burton, M. J. Lalor, and M. A. Gdeisat, *Appl. Opt.* **41**, 7437 (2002).
29. T. Weitkamp, A. Diaz, B. Nöhammer, F. Pfeiffer, M. Stupanoni, E. Ziegler, and C. David, *Proc. SPIE* **5533**, 140 (2004).
30. H. Ohashi, M. Yabashi, K. Tono, Y. Inubushi, T. Sato, T. Togashi, Y. Senba, T. Koyama, H. Yumoto, K. Miyokawa, T. Ohsawa, S. Goto, and T. Ishikawa, *Nucl. Instrum. Meth. A* **710**, 139 (2013).